Constraining new physics from Higgs measurements with Lilith: update to LHC Run 2 results

Thi Nhung Dao[1], Sabine Kraml[2*], Duc Ninh Le[1], Loc Tran Quang[1]

1 Institute For Interdisciplinary Research in Science and Education, ICISE, 590000, Quy Nhon, Vietnam
2 Laboratoire de Physique Subatomique et de Cosmologie, Université Grenoble-Alpes, CNRS/IN2P3, 53 Avenue des Martyrs, F-38026 Grenoble, France
* sabine.kraml@lpsc.in2p3.fr

June 15, 2019

Abstract

Lilith is public python library for constraining new physics from Higgs signal strength measurements. We here present version 2.0 of Lilith together with an updated database which includes the full set of ATLAS and CMS Run 2 Higgs results for 36 fb^{-1}. Both the code and the XML database where extended from the ordinary Gaussian approximation employed in Lilith-1.1 to using variable Gaussian and Poisson distributions. Moreover, Lilith can now make use of correlation matrices of arbitrary dimension. We provide detailed validations of the implemented experimental results as well as a status of global fits for *i)* reduced Higgs couplings and *ii)* Two-Higgs-doublet models of Type-I and Type-II. Lilith-2.0 is available on GitHub and ready to be used to constrain a wide class of new physics scenarios.

1 Introduction

Introduce Higgs couplings fits and `Lilith` [1] .....
.....
.....
.....
.....
.....
.....

2 Extended XML format for experimental input

In the `Lilith` database, every single experimental result is stored in a separate XML file. This allows to easily select the results to use in a fit, and it also makes maintaining and updating the database rather easy.

The root tag of each XML file is `<expmu>`, which has two mandatory attributes, `dim` and `type` to specify the type of signal strength result. Production and decay modes are specified via `prod` and `decay` attributes either directly in the `<expmu>` tag or as efficiencies in `<eff>` tags. Additional (optional) information can be provided in `<experiment>`, `<source>`, `<sqrts>`, `<CL>` and `<mass>` tags. Taking the $H \to \gamma\gamma$ result from the combined ATLAS and CMS Run 1 analysis [2] as a concrete example, the structure of the XML file is

```
<expmu decay="gammagamma" dim="2" type="n">
  <experiment>ATLAS-CMS</experiment>
  <source type="publication">CMS-HIG-15-002; ATLAS-HIGG-2015-07</source>
  <sqrts>7+8</sqrts>
  <mass>125.09</mass>
  <CL>68%</CL>

  <eff axis="x" prod="ggH">1.</eff>
  <eff axis="y" prod="VVH">1.</eff>

  <!-- (...) -->
</expmu>
```

where `<!-- (...) -->` is a placeholder for the actual likelihood information. For a detailed description, we refer to the original `Lilith` manual [1]. In the following, we assume that the reader is familiar with the basic syntax.

So far, the likelihood information could be specified in one or two dimensions in the form of [1]: 1D intervals given as best fit with 1σ error; 2D likelihood contours described as best fit point and parameters a, b, c which parametrize the inverse of the covariance matrix; or full likelihood information as 1D or 2D grids of $-2\log L$. The first two options, 1D intervals and 2D likelihood contours, declared as `type="n"` in the `<expmu>` tag, employ an ordinary Gaussian approximation; in the 1D case, asymmetric errors are accounted for by putting together two one-sided Gaussians with the same mean but different variances, while the 2D case assumes symmetric errors. This does does not always allow to describe the experimental data (i.e. the true likelihood) very well. Full 2D likelihood grids would be much better but are rarely available.

In order to treat asymmetric uncertainties in a better way, we have extended the XML format and fitting procedure in `Lilith` to Gaussian distributions of variable width ("variable Gaussian") as well as generalized Poisson distributions. The declaration is `type="vn"` for variable Gaussian or `type="p"` for Poisson distribution in the `<expmu>` tag. Both work for 1D and 2D data with the same syntax. Moreover, in order to make use of the N-dimensional ($N > 2$) correlation matrices which both ATLAS and CMS have started to provide, we have added a new XML format for correlated signal strengths in more than two dimensions. This can be used with the ordinary or variable Gaussian approximation for the likelihood. In the following we give explicit examples for the different possibilities.

1D likelihood parameterization

For 1D data, the format remains the same as in [1]. For example, a signal strength $\mu(ZH,\, b\bar{b}) = 1.12^{+0.50}_{-0.45}$ is implemented as

```
<bestfit>1.12</bestfit>
<param>
  <uncertainty side="left">-0.45</uncertainty>
  <uncertainty side="right">0.50</uncertainty>
</param>
```

The `<bestfit>` tag contains the best-fit value, while the `<uncertainty>` tag contains the left (negative) and right (positive) 1σ errors.[1] The choice of likelihood function is done by setting `type="n"` for ordinary, 2-sided Gaussian (as in `Lilith-1.1`); `type="vn"` for a variable Gaussian; or `type="p"` for a Poisson distribution in the `<expmu>` tag.

2D likelihood parameterization

For `type="vn"` and `type="p"`, signal strengths in 2D with a correlation are now described in an analogous way as 1D data. For example, $\mu(\mathrm{ggH}, WW) = 1.10^{+0.21}_{-0.20}$ and $\mu(\mathrm{VBF}, WW) = 0.62^{+0.36}_{-0.35}$ with a correlation of $\rho = -0.08$ can be implemented as

```
<expmu decay="WW" dim="2" type="vn">

  <eff axis="x" prod="ggH">1.0</eff>
  <eff axis="y" prod="VBF">1.0</eff>

  <bestfit>
    <x>1.10</x>
    <y>0.62</y>
  </bestfit>

  <param>
    <uncertainty axis="x" side="left">-0.20</uncertainty>
    <uncertainty axis="x" side="right">+0.21</uncertainty>
    <uncertainty axis="y" side="left">-0.35</uncertainty>
    <uncertainty axis="y" side="right">+0.36</uncertainty>
    <correlation>-0.08</correlation>
  </param>
</expmu>
```

Here, the `<eff>` tag is used to declare the `x` and `y` axes. The `<bestfit>` tag specifies the location of the best-fit point in the (`x`,`y`) plane. The `<uncertainty>` tags contain the left (negative) and right (positive) 1σ errors for the `x` and `y` axes, and finally the `<correlation>` tag specifies the correlation between `x` and `y`. The choice of likelihood function is again done by setting `type="vn"` or `type="p"` in the `<expmu>` tag.

To ensure backwards compatibility, `type="n"` however still requires the tags `<a>`, `<b>`, `<c>` to give the inverse of the covariance matrix instead of `<uncertainty>` and `<correlation>`, see [1].

[1] The values in the `<uncertainty>` tag can be given with or without a sign.

Multi-dimensional data

For correlated signal strengths in more than 2 dimensions, a new format is introduced. We here illustrate it by means of the CMS result [3], which has signal strengths for 24 production and decay mode combinations plus a 24×24 correlation matrix. First, we set `dim="24"` and label the various signal strengths as axes d1, d2, d3, ... d24:[2]

```
<expmu dim="24" type="vn">
  <eff axis="d1" prod="ggH" decay="gammagamma">1.0</eff>
  <eff axis="d2" prod="ggH" decay="ZZ">1.0</eff>
  <eff axis="d3" prod="ggH" decay="WW">1.0</eff>
  ...
  <eff axis="d24" prod="ttH" decay="tautau">1.0</eff>
```

The best-fit values for each axis are specified as

```
  <bestfit>
    <d1>1.16</d1>
    <d2>1.22</d2>
    <d3>1.35</d3>
    ...
    <d24>0.23</d24>
  </bestfit>
```

The `<param>` tag then contains the uncertainties and correlations in the form

```
  <param>
    <uncertainty axis="d1" side="left">-0.18</uncertainty>
    <uncertainty axis="d1" side="right">+0.21</uncertainty>
    <uncertainty axis="d2" side="left">-0.21</uncertainty>
    <uncertainty axis="d2" side="right">+0.23</uncertainty>
    ...
    <uncertainty axis="d24" side="left">-0.88</uncertainty>
    <uncertainty axis="d24" side="right">+1.03</uncertainty>

    <correlation entry="d1d2">0.12</correlation>
    <correlation entry="d1d3">0.16</correlation>
    <correlation entry="d1d4">0.08</correlation>
    ...
    <correlation entry="d23d24">0</correlation>
  </param>
</expmu>
```

This will also work for `type="n"`.

[2] The `<experiment>`, `<source>`, `<sqrts>`, etc. tags are omitted for brevity.

3 Likelihood calculation

The statistic procedure used in `Lilith` was described in details in [1]. The main quantity given as an output is the $-2\log L$ which is computed according to the four different types of experimental data: 1D interval, 1D full, 2D contour, 2D full. Except for the full profile likelihoods, the $-2\log L$ values are computed using the ordinary Gaussian distribution approximation. Since we have found that this assumption does not describe very well data in many cases, therefore we have added the variable Gaussian and generalised Poison distributions. We have also extended the code to include the multi-dimensional data. In this section we present in details how the $-2\log L$ quantities are computed according to the two distribution approximations. For the old implementation of the ordinary Gaussian distribution in `Lilith` we refer the reader to [1]. In the code, computations of $-2\log L$ are implemented in `computelikelihood.py`.

The variable Gaussian distribution

As shown in [4], variable Gaussian distribution is one of good approximations to deal with asymmetric uncertainties. We apply the "Variable Gaussian (2)" in Section 3.6 of [4]. In the 1D interval case, the likelihood is given by

$$-2\log L(\mu) = \frac{(\mu-\hat{\mu})^2}{\sigma^+\sigma^- + (\sigma^+-\sigma^-)(\mu-\hat{\mu})}, \tag{1}$$

where $\hat{\mu}$ denotes the best-fit signal strength, and σ^- and σ^+ are the left and right uncertainties at 68% CL, respectively. Note that $\hat{\mu}, \sigma^-, \sigma^+$ are taken directly from experimental papers or fitted if they are not given explicitly. If not stated otherwise, these notations are used for the entire section. The ordinary Gaussian distribution is obtained with $\sigma^+ = \sigma^-$. The likelihood using variable Gaussian however has a singularity point at

$$\mu = \hat{\mu} - \frac{\sigma^+\sigma^-}{\sigma^+ - \sigma^-}. \tag{2}$$

This may happens if the values of reduced couplings may be two large and unphysical. In the case of n dimension data ($n > 1$), we use the $n \times n$ correlation matrix given by the experimental collaboration, if it is available, together with the best fit points and the left and right uncertainties at 68% CL. Especially when data are given in terms of two dimensional contour plots, we can use also variable Gaussian to fit for the correlation and the best fit point and their uncertainties at 68 % CL, if they are not given explicitly by the experimental collaboration. For the n dimensional signal strength vector $\boldsymbol{\mu} = (\mu_1, \ldots, \mu_n)$, the likelihood reads

$$-2\log L(\boldsymbol{\mu}) = (\boldsymbol{\mu}-\hat{\boldsymbol{\mu}})^T C^{-1} (\boldsymbol{\mu}-\hat{\boldsymbol{\mu}}), \tag{3}$$

where the best fit point $\hat{\boldsymbol{\mu}} = (\hat{\mu}_1, \ldots, \hat{\mu}_n)$ and the covariance matrix is constructed from the correlation matrix ρ as

$$C = \boldsymbol{\Sigma}(\boldsymbol{\mu}).\rho.\boldsymbol{\Sigma}(\boldsymbol{\mu}), \quad \boldsymbol{\Sigma}(\boldsymbol{\mu}) = \mathrm{diag}(\Sigma_1, \ldots, \Sigma_n) \tag{4}$$

with

$$\Sigma_i = \sqrt{\sigma_i^+\sigma_i^- + (\sigma_i^+ - \sigma_i^-)(\mu_i - \hat{\mu}_i)}, \quad i = 1, \ldots, n. \tag{5}$$

Here the σ_i^- and σ_i^+ are the left and right uncertainties at 68% CL of the ith combination of production and decay channel, respectively. For the multi-dimensional data in the ordinary

Gaussian distribution, the relation between covariance matrix and the correlation matrix becomes

$$C = \frac{1}{4}[\boldsymbol{\sigma}^{+} + \boldsymbol{\sigma}^{-}].\rho.[\boldsymbol{\sigma}^{+} + \boldsymbol{\sigma}^{-}], \tag{6}$$

where $\boldsymbol{\sigma}^{+} = \mathrm{diag}(\sigma_1^{+}, \ldots, \sigma_n^{+})$ and $\boldsymbol{\sigma}^{-} = \mathrm{diag}(\sigma_1^{-}, \ldots, \sigma_n^{-})$.

The generalised Poison distribution

We apply the generalised Poison distribution for one and two dimensional data. For the one dimensional data, the likelihood is implemented according to "Generalised Poisson" of [4],

$$\log L(\mu) = -\nu\gamma(\mu - \hat{\mu}) + \nu \log\left[1 + \gamma\left(\mu - \hat{\mu}\right)\right], \tag{7}$$

where γ and ν are solved numerically from the following equations

$$\frac{1 - \gamma\sigma^{-}}{1 + \gamma\sigma^{+}} = e^{-\gamma(\sigma^{+} + \sigma^{-})}, \quad \nu = \frac{1}{2(\gamma\sigma^{+} - \log(1 + \gamma\sigma^{+}))}. \tag{8}$$

For the two dimensional data, we use the conditioning bivariate Poison distribution described in [5], that has no restriction on the sign and magnitude of the correlation ρ. The joint distribution is a product of a marginal and a conditional distribution. The decision of which channel belongs to the marginal or the conditional distribution is based on the validation plots. To illustrate our formulae, we assume that the data of the channel X follows the marginal distribution while data of the channel Y belongs to the conditional distribution. The joint log-likelihood is the the sum of the marginal and conditional log-likelihoods

$$\log L(\mu_X, \mu_Y) = \log L(\mu_X) + \log L(\mu_Y|\mu_X), \tag{9}$$

where the marginal likelihood for the channel X is given by

$$\log L(\mu_X) = -\nu_X\gamma_X(\mu_X - \hat{\mu}_X) + \nu_X \log\left[1 + \gamma_X\left(\mu_X - \hat{\mu}_X\right)\right], \tag{10}$$

and the conditional likelihood for the channel Y given the channel X

$$\log L(\mu_Y|\mu_X) = f(\mu_X, \mu_Y) - f(\hat{\mu}_X, \hat{\mu}_Y) + \nu_Y \log\frac{f(\mu_X, \mu_Y)}{f(\hat{\mu}_X, \hat{\mu}_Y)}. \tag{11}$$

Here the function f reads

$$f(a, b) = -\nu_Y\gamma_Y\left(b - \hat{\mu}_Y + \frac{1}{\gamma_Y}\right)\exp\left[\nu_X\alpha - \left(e^{\alpha} - 1\right)\nu_X\gamma_X(a - \hat{\mu}_X + \frac{1}{\gamma_X})\right], \tag{12}$$

where α is solved numerically from the correlation expression

$$\rho = \frac{\nu_X\nu_Y\left(e^{\alpha} - 1\right)}{\sqrt{\nu_X\nu_Y\left[1 + \nu_Y\left(e^{\nu_X(e^{\alpha} - 1)^2} - 1\right)\right]}}, \tag{13}$$

and the γ_x, ν_X and γ_Y, ν_Y are solutions of the Eq. 8 for the X and Y channels, respectively.

4 ATLAS and CMS results included in the database update

4.1 ATLAS Run 2 results for 36 fb^{-1}

The ATLAS Run 2 results included in this release are summarised in Table 1 and explained in more detail below.

mode	$\gamma\gamma$	ZZ^*	WW^*	$\tau\tau$	$b\bar{b}$	inv.
ggH	[6]	[7]	[8]	[9]	–	–
VBF	[6]	[7]	[8]	[9]	[10]	–
WH	[6]	[7]	–	–	[11]	–
ZH			–	–	[11]	[12]
ttH	[6,13]	[7,13]	[13]	[13]	[13,14]	–

Table 1: Overview of ATLAS Run 2 results included in this release.

***H* → γγ (HIGG-2016-21):** The ATLAS analysis [6] provides in Fig. 12 $H \to \gamma\gamma$ signal strengths separated into ggH, VBF, VH and "top" (ttH+tH) production modes. Since no correlations are given for the signal strengths, we use instead the correlations for the stage-0 simplified template cross sections (STXS) provided in Fig. 40a of the ATLAS paper, which should be a close enough match. It turns out that these data do not allow to reproduce very well the ATLAS coupling fits for (C_V, C_F) or (C_γ, C_g). The reason seems to be that the μ values rounded to one decimal are not precise enough. We have therefore extracted the best-fit points and uncertainties from the 1D profile likelihoods, which are provided as Auxiliary Figures 23a–d on the analysis webpage, as[3] $\mu(\text{ggH}, \gamma\gamma) \simeq 0.81^{+0.19}_{-0.18}$, $\mu(\text{VBF}, \gamma\gamma) \simeq 2.04^{+0.61}_{-0.53}$, $\mu(\text{VH}, \gamma\gamma) \simeq 0.66^{+0.89}_{-0.80}$ and $\mu(\text{ttH}, \gamma\gamma) \simeq 0.54^{+0.64}_{-0.55}$ (using a Poisson likelihood). These numbers are consistent with the rounded values in Fig. 12 of [6], but using more digits improves the coupling fits as shown in Fig. 1.

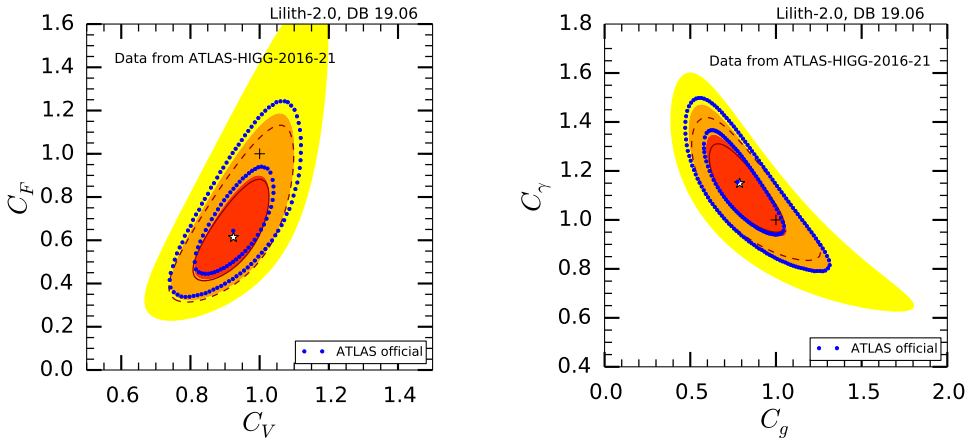

Figure 1: Fit of C_F vs. C_V (left) and C_γ vs. C_g (right) for data from the ATLAS $H \to \gamma\gamma$ analysis [6]. The red, orange and yellow filled areas show the 68%, 95% and 99.7% CL regions obtained with `Lilith` using best-fit values and uncertainties for the signal strengths as extracted from Aux. Figs. 23a–d of the ATLAS analysis together with the 4×4 correlation matrix for the stage-0 STXS. This can be compared to the 68%, 95% CL contours obtained using the rounded values from Fig. 12 of [3] (solid and dashed dark red lines) and to the official 68% and 95% CL contours from ATLAS (blue dots).

[3] In the XML file we use the exact numbers from the fit to the 1D profile likelihoods.

225 ***H → ZZ* → 4l* (HIGG-2016-22):** A similar issue as discussed for $H \to \gamma\gamma$
226 above arises for $H \to ZZ^*$, see the left panel in Fig. 2. Here we used the ggH and VBF
227 signal strengths given in Table 9 of [7] with correlation $\rho = -0.41$ as of Aux. Fig. 4c,
228 assuming a Poisson likelihood. (This is a case were the variable Gaussian approximation
229 performs less well). For the VH and ttH production modes, lacking more information, we
230 converted the given 95% CL limits into $\mu(\text{VH}, ZZ^*) = 0^{+1.85}_{-0}$ and $\mu(\text{ttH}, ZZ^*) = 0^{+3.75}_{-0}$
231 using a 1-sided Gaussian. The result is clearly not satisfactory. The closest match of
232 the official CL contours is obtained if we fit the 1D profile likelihoods for $\mu(\text{ggH}, ZZ^*)$
233 and $\mu(\text{VBF}, ZZ^*)$ shown in Aux. Figs. 7a and 7b of [7] as Poisson distributions. This
234 gives $\mu(\text{ggH}, ZZ^*) \simeq 1.12^{+0.25}_{-0.22}$ and $\mu(\text{VBF}, ZZ^*) \simeq 3.88^{+1.75}_{-1.46}$, which we implement as a
235 bivariate Poisson distribution with correlation $\rho = -0.41$ (from Aux. Fig. 4c of [7]). The
236 VH and ttH production modes are treated as before. As shown in the right panel of Fig. 2,
237 this allows to reproduce reasonably well the C_F vs. C_V fit from the ATLAS paper.

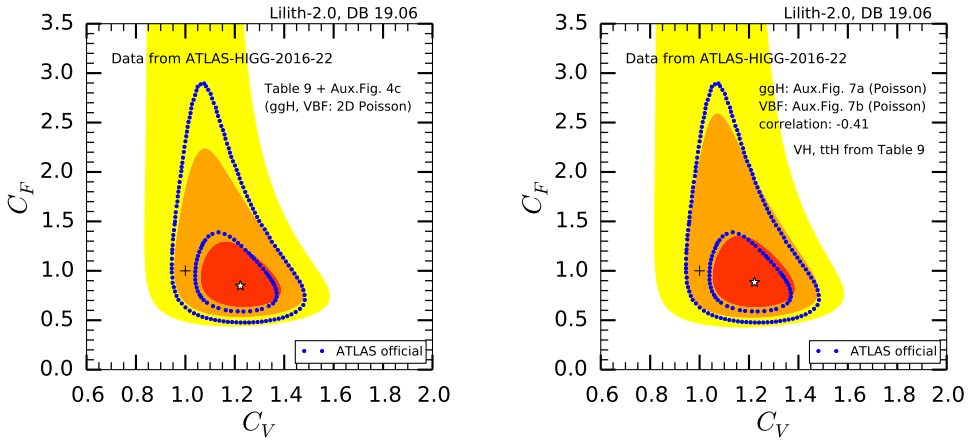

Figure 2: Fit of C_F vs. C_V for data from the ATLAS $H \to ZZ^*$ analysis, on the left using the values from Table 9 of [7], on the right using $\mu(\text{ggH}, ZZ^*)$ and $\mu(\text{VBF}, ZZ^*)$ as fitted from Aux. Figs. 7a and 7b of [7]. In both panels, the ggH vs. VBF likelihood is approximated as a bivariate Poissonian with correlation −0.41. The 68%, 95% and 99.7% CL regions obtained with `Lilith` are shown as red, orange and yellow areas, and compared to the 68% and 95% CL contours from ATLAS (in blue).

238 ***H → WW* → 2l2ν* (HIGG-2016-07):** Ref. [8] focusses on the measurement of
239 the inclusive ggH and VBF Higgs production cross sections in the $H \to WW^* \to e\nu\mu\nu$
240 channel. The paper quotes on page 13 signal strengths of $\mu(\text{ggH}, WW) = 1.10^{+0.21}_{-0.20}$ and
241 $\mu(\text{VBF}, WW) = 0.62^{+0.36}_{-0.35}$. We implemented these as a 2D result with a correlation of
242 $\rho = -0.08$ using the variable Gaussian approximation; the correlation was fitted from the
243 $\sigma \times \text{BR}$ plot, Fig. 9, of [8]. No coupling fits are available which could be used for validation.
244
245 ***H → ττ* (HIGG-2017-07):** This ATLAS cross section measurement in the $H \to \tau\tau$
246 channel [9] provides as Aux. Fig. 5 the 68% and 95% CL contours in the $\mu(\text{ggH}, \tau\tau)$ vs.
247 $\mu(\text{VBF}, \tau\tau)$ plane. A fit of a bivariate variable Gaussian to the 95% CL contour in this
248 plot gives $\mu(\text{ggH}, \tau\tau) \simeq 1.0^{+0.72}_{-0.59}$ and $\mu(\text{VBF}, WW) = 1.20^{+0.62}_{-0.56}$ with $\rho = -0.45$, which
249 are the values implemented in the database. As no other validation material is available,
250 we show in Fig. 3 our reconstruction of the experimental likelihood in the $\mu(\text{ggH}, \tau\tau)$ vs.
251 $\mu(\text{VBF}, \tau\tau)$ plane. Note that a fit to the 68% CL contour of ATLAS gives a less good result.
252

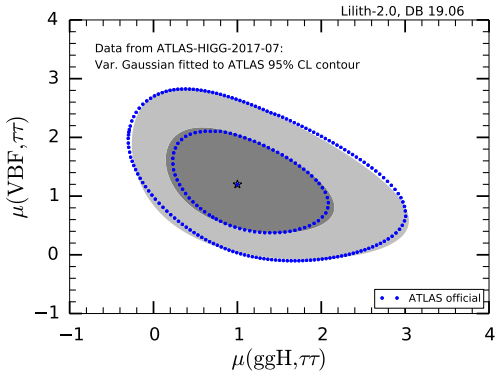

Figure 3: Reconstruction of the experimental likelihood in the $H \to \tau\tau$ channel from [9] as 2D variable Gaussian in the $\mu(\text{ggH}, \tau\tau)$ vs. $\mu(\text{VBF}, \tau\tau)$ plane. The 68% and 95% CL regions obtained with `Lilith` are shown in dark and light gray, respectively, and compared to the 68% and 95% CL contours from ATLAS (in blue).

***$H \to b\bar{b}$* (HIGG-2016-29 and HIGG-2016-30):** For the $H \to b\bar{b}$ decay mode, ATLAS gives $\mu(\text{ZH}, b\bar{b}) = 1.12^{+0.50}_{-0.45}$, $\mu(\text{WH}, b\bar{b}) = 1.35^{+0.68}_{-0.59}$ [10] and $\mu(\text{VBF}, b\bar{b}) = 3.0^{+1.7}_{-1.6}$ [10]. No correlation data is available, so we implemented each of these as a 1D result; a Poisson likelihood is assumed per default.

ttH production (HIGG-2017-02): The ATLAS paper [13], reporting evidence for $t\bar{t}H$ production, provides in Fig. 16 the signal strength results broken down into $H \to \gamma\gamma$, VV ($= ZZ^* + WW^*$), $\tau\tau$ and $b\bar{b}$ decay modes from a combined analysis of all $t\bar{t}H$ searches. Correlations are not given explicitly but can be estimated from Figs. 17a and 17b in [13] as $\rho(b\bar{b}, VV) \simeq 0.04$ for the correlation between the $H \to b\bar{b}$ and $H \to VV$ decay modes and $\rho(\tau\tau, VV) \simeq -0.35$ for that between the $H \to \tau\tau$ and $H \to VV$ decay modes. In Fig. 4, we compare the C_F vs. C_V fit from the implementation in `Lilith` to the official one from [13]. While the agreement is not very good, one has to note that without the correlations quoted above the situation is much worse.

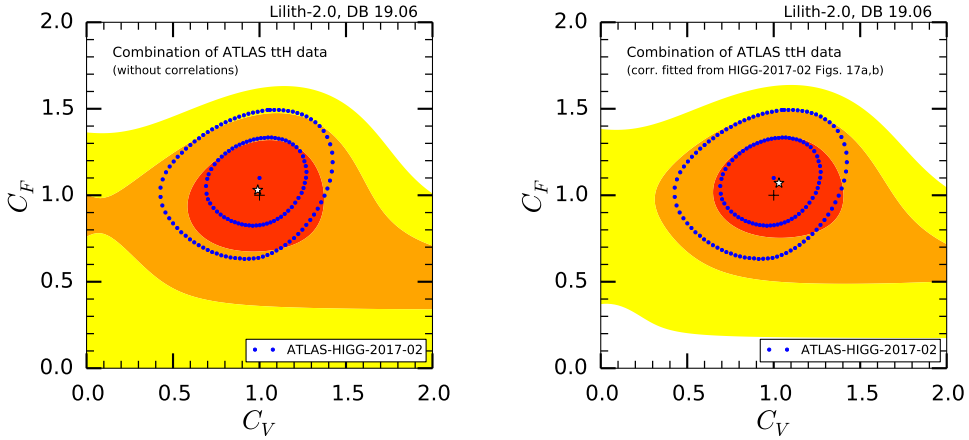

Figure 4: Fit of C_F vs. C_V from a combination of the ATLAS ttH measurements, on the left without and on the right with the correlations fitted from Figs. 17a,b in [13] (see text for details). The 68%, 95% and 99.7% CL regions obtained with `Lilith` are shown as red, orange and yellow areas, and compared to the 68%, 95% CL contours from ATLAS (in blue).

A few comments are in order here. First, the measurement of $\mu(\mathrm{t\bar{t}H},\, \gamma\gamma)$ actually comes from [6] (HIGG-2016-21, see above) and is also included in the HIGG-2016-21 XML file; to avoid overlap when using both the HIGG-2016-21 and HIGG-2017-02 datasets, we provide a 3D XML file for the latter which includes only the VV, $\tau\tau$ and $b\bar{b}$, but not the $\gamma\gamma$, decay modes. Second, the individual measurement [14] gives $\mu(\mathrm{t\bar{t}H},\, b\bar{b})$ to two decimals $(0.84^{+0.64}_{-0.61})$ instead just one (0.8 ± 0.6) in [13]. Since this makes a visible difference in Fig. 4, improving the quality of the fit, we use the more precise numbers from [14]. Third, for $\mu(\mathrm{t\bar{t}H},\, VV)$ the contribution from $H \to WW^*$ should dominate, but the concrete weights of the ZZ^* and WW^* decay modes are not given in [13]. This is not a problem as long as $C_Z = C_W \equiv C_V$, but one should not use the HIGG-2017-02 XML file for any other case.

***H* → invisible (HIGG-2016-28):** Results from the search for invisibly decaying Higgs bosons produced in association with a Z boson are presented in [12]. A 95% CL upper limit of $\mathrm{BR}(H \to \mathrm{inv.}) < 0.67$ is set for $m_H = 125$ GeV assuming the SM ZH production cross section. In the `Lilith` database, we use a likelihood grid as function $\mathrm{BR}(H \to \mathrm{inv.})$ extracted from Aux. Fig. 1c on the analysis' webpage.

4.2 CMS Run 2 results for 36 fb^{-1}

The CMS Run 2 results included in this release are summarised in Table 2 and explained in more detail below.

mode	$\gamma\gamma$	ZZ^*	WW^*	$\tau\tau$	$b\bar{b}$	$\mu\mu$	inv.
ggH	[3]	[3]	[3]	[3]	[3]	[3]	[15]
VBF	[3]	[3]	[3]	[3]	–	[3]	[15]
WH	[3]	[3]	[3]	[16]	[3]	–	[15]
ZH	[3]	[3]	[3]	[16]	[3]	–	[15]
ttH	[3]	[3]	[3]	[3]	[3]	–	–

Table 2: Overview of CMS Run 2 results included in this release. Note that we use the full 24×24 correlation matrix for the signal strengths for each production and decay mode combination provided in [3].

Combined measurements (HIG-17-031): CMS presented in [3] a combination of the individual measurements for the $H \to \gamma\gamma$ [17], ZZ [18], WW [19], $\tau\tau$ [20], $b\bar{b}$ [21,22] and $\mu\mu$ [23] decay modes as well as the $t\bar{t}H$ analyses [24–26]. We use the best fit values and uncertainties for the signal strengths for each production and decay mode combination presented in Table 3 of [3] together with the 24×24 correlation matrix provided as "Additional Figure 1" on the analysis webpage. As shown in Figs. 5 and 6, this allows to reproduce well the coupling fits of the CMS paper.

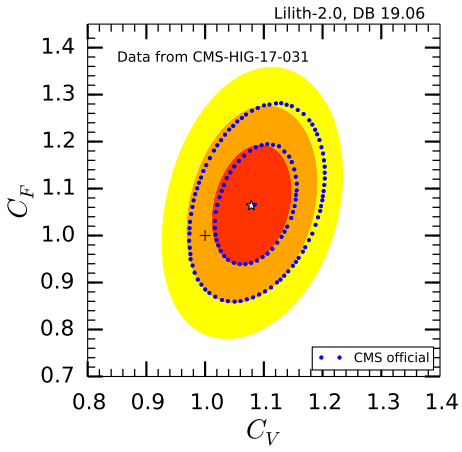

Figure 5: Fit of C_F vs. C_V using best-fit values and uncertainties for the signal strengths for each production (ggH, VBF, WH, ZH, ttH) and decay ($\gamma\gamma$, ZZ, WW, $\tau\tau$, $b\bar{b}$, $\mu\mu$) mode combination together with the 24×24 correlation matrix from the CMS combination paper [3]. The 1σ, 2σ and 3σ regions obtained with `Lilith` are shown as red, orange and yellow areas, and compared to the 1σ and 2σ contours from CMS (blue dots).

***VH*, $H \to \tau\tau$ (HIG-18-007)**: The above data from [3] is supplemented by the results for the $\tau\tau$ decay mode from the WH and ZH targeted analysis [16]. These are implemented in the form of 1D intervals for $\mu(ZH,\ H \to \tau\tau)$ and $\mu(WH,\ H \to \tau\tau)$ taken from Fig. 6 of [16].

***H* → invisible (HIG-17-023)**: In [15], CMS performed a search for invisible decays of a Higgs boson produced through vector boson fusion. We use the profile likelihood ratios for the qqH-tag, Z(ll)H-, V(qq')H- and ggH-tag categories extracted from their Fig. 8b

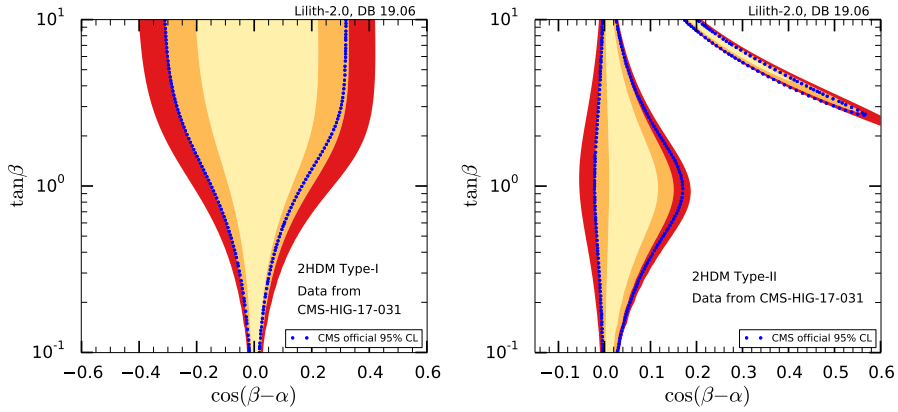

Figure 6: Fit of $\tan\beta$ vs. $\cos(\beta-\alpha)$ for the Two-Higgs-Doublet models of Type I (left) and Type II (right) using the data from the combined CMS measurement [3]. The beige, orange and red filled areas show the 68%, 95% and 99.7% CL regions obtained with `Lilith`, while the blue dots mark the 95% CL contours from CMS.

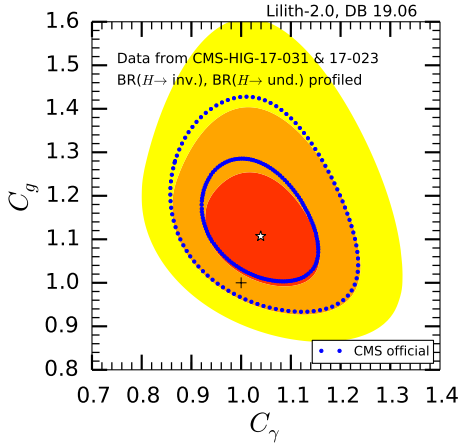

Figure 7: Fit of C_g vs. C_γ using the data from the combined CMS measurement [3] and the search for invisible decays of a Higgs boson [15]. The branching ratios of invisible and undetected decays are treated as free parameters in the fit. The 1σ, 2σ and 3σ regions obtained with `Lilith` are shown as red, orange and yellow areas, and compared to the 1σ and 2σ contours from CMS (in blue).

together with the relative contributions from the different Higgs production mechanisms given in Table 6 of that paper. This assumes that the relative signal contributions stay roughly the same as for SM production cross sections. For validation, we reproduce in Fig. 7 the C_g vs. C_γ fit of [3], where the branching ratios of invisible and undetected decays are treated as free parameters.[4]

[4] The profiling in Fig. 7 was done with `Minuit`. Since `Minuit` does not allow conditional limits, in this case $\mathrm{BR}(H \to \text{inv.}) + \mathrm{BR}(H \to \text{undetected}) < 1$, we demanded that both $\mathrm{BR}(H \to \text{inv.})$ and $\mathrm{BR}(H \to \text{undetected})$ be less than 50%.

5 Status of Higgs coupling fits

6 Conclusion

must include a conclusion.

Acknowledgements

S.K. thanks W. Adam, R. Schöfbeck, W. Waltenberger and N. Wardle for helpful discussions. This work was supported in part by the IN2P3 theory project "LHC-itools: methods and tools for the interpretation of the LHC Run 2 results for new physics". D.T.N. thanks the LPSC Grenoble for hospitality and financial support for a research visit within the LHC-itools project. L.T.Q. thanks the ICISE ...

A Overview of XML data files

B Implementation of 2D Poisson likelihood with correlation

B.1 Log-likelihood for Poisson distribution with continuous variable

The probability mass function of Poisson distribution, with parameter $\lambda > 0$, and variable $k = 0, 1, 2, 3, ...$:

$$f(k;\lambda) = \frac{e^{-\lambda}\lambda^k}{k!}. \tag{14}$$

The log-likelihood function for Poisson distribution:

$$l(\lambda;k) = \log[f(k;\lambda)] = -\lambda + k\log\lambda - \log k!. \tag{15}$$

Here, since k is a discrete variable, we would redefine a log-likelihood function of parameter λ that fix continuous variable, denoted as "ν". We re-define the parameter as $\lambda \equiv \rho(\lambda - c) + \tau$, with $\eta = \tau/\rho$, and c is the expected value at which the log-likelihood function reaches extrema. The new log-likelihood function reads:

$$l(\lambda;\nu) = -\rho(\lambda - c + \eta) + \nu\log\rho(\lambda - c + \eta) + \text{const.} \tag{16}$$

Here we want to set the extrema at $\lambda = c$. Since the Poisson distribution has expected value equal it parameter, we set $\nu = \rho\eta$ so that the log-likelihood function reaches extrema at $f(c)$. For Poisson distribution, the extrema of log-likelihood function is not equal 0, we will consider its Δ log-likelihood function:

$$\Delta l(\lambda;\nu) = l(\lambda;\nu) - l(c;\nu) = -\rho(\lambda - c) + \nu\ln\left[1 + \frac{\rho}{\nu}(\lambda - c)\right]. \tag{17}$$

$\Delta l(\sigma_-;\nu)$ and $\Delta l(\sigma_+;\nu)$ yields $-1/2$, dividing their r.h.s terms of by ν followed by taking the exponentials, we get the relation:

$$\frac{1 - \gamma\sigma_-}{1 - \gamma\sigma_+} = e^{-\gamma(\sigma_- + \sigma_+)}. \tag{18}$$

From $\Delta l(\sigma_+;\nu) = -1/2$, we could derive ν:

$$\nu = \frac{1}{2(\gamma\sigma_+ - \ln(1 + \gamma\sigma_+))}. \tag{19}$$

B.2 A model for bivariate Poisson distribution with negative correlation

For references, see: Berkhout, Plug's.
The probability mass function (pmf) of Poisson distribution, with parameter $\lambda > 0$, and variable $k = 0, 1, 2, 3, ...$:

$$f(k;\lambda) = \frac{e^{-\lambda}\lambda^k}{k!}. \tag{20}$$

We would like to apply a model of bivariate Poisson distribution which allows negative correlation. We define marginal and dependent pmf respectively as:

$$g_1(k_1;\lambda_1) = \frac{e^{-\lambda_1}\lambda_1^{k_1}}{k_1!}, \tag{21}$$

$$g_2(k_2|k_1;\lambda_2) = \frac{e^{-\lambda_2}\lambda_2^{k_2}}{k_2!}. \tag{22}$$

By convention, the parameters read:

$$\lambda_1 = e^{x'\beta_1}, \tag{23}$$

$$\lambda_2 = e^{x'\beta_2+\alpha k_1}. \tag{24}$$

The parameter α is added as a small correction that correspondent for the correlation of k_1, k_2. The joint pmf:

$$f(k_1,k_2;\lambda_1,\lambda_2) = g_2(k_2|k_1;\lambda_2)g_1(k_1;\lambda_1). \tag{25}$$

The marginal pmf remains the form of Poisson distribution, its expected value and variance reads:

$$E(k_1) = \mathrm{Var}(k_1) = \lambda_1. \tag{26}$$

The (r, s)th factorial moment of the joint distribution is derived as:

$$E\left[k_1(k_1-1)...(k_1-r+1)k_2(k_2-1)...(k_2-s+1)\right] \tag{27}$$

$$= \sum_{k_1=r}^{\infty}\sum_{k_2=s}^{\infty} \frac{e^{k_1(x'\beta_1)-\exp(x'\beta_1)+k_2(x'\beta_2+\alpha k_1)-\exp(x'\beta_2+\alpha k_1)}}{(k_1-r)!(k_2-s)!} \tag{28}$$

$$= \lambda_1^r e^{\lambda_1[\exp(s\alpha)-1]+sx'\beta_2+rs\alpha}. \tag{29}$$

The expected value, variance of k_2 and expected value of k_1k_2 is derived from the factorial moment 29 as:

$$E(k_2) = e^{x'\beta_2+(\exp(\alpha)-1)\lambda_1}, \tag{30}$$

$$\mathrm{Var}(k_2) = E(k_2) + [E(k_2)]^2\{e^{\lambda_1[\exp(\alpha)-1]}\}, \tag{31}$$

$$E(k_1k_2) = \lambda_1 E(k_2)\exp(\alpha). \tag{32}$$

The covariance of k_1 and k_2 reads:

$$\mathrm{Cov}(k_1,k_2) = E(k_1k_2) - E(k_1)E(k_2) = \lambda_1 E(k_2)[\exp(\alpha)-1]. \tag{33}$$

The correlation reads:

$$\mathrm{Corr}(k_1,k_2) = \frac{\lambda_1 E(k_2)[\exp(\alpha)-1]}{\sqrt{\lambda_1 E(k_2)\{1+E(k_2)\{e^{\lambda_1[\exp(\alpha)-1]^2}-1\}\}}}. \tag{34}$$

For later convenience, we derive the relation between λ_2 and $E(k_2)$:

$$\lambda_2 = E(k_2)e^{\alpha k_1-[\exp(\alpha)-1]\lambda_1} = E(k_2)e^{\alpha k_1-[\exp(\alpha)-1]E(k_1)}. \tag{35}$$

B.3 Log-likelihood for bivariate Poisson distribution with continuous variable and negative correlation

We derive a log-likelihood function that fixes continuous variables for the bivariate Poisson distribution which allows negative correlation. Now for the marginal pmf:

$$g_1(k_1;\lambda_1) = \frac{e^{-\lambda_1}\lambda_1^{k_1}}{k_1!}. \tag{36}$$

It remains the form of ordinary Poisson distribution. We apply 17 to derive the Δ log-likelihood function:

$$\Delta l_1(\lambda_1;\nu_1) = -\rho_1(\lambda_1 - c_1) + \nu_1 \log\left[1 + \frac{\rho_1}{\nu_1}(\lambda_1 - c_1)\right]. \tag{37}$$

Considering the dependent pmf:

$$g_2(k_2|k_1;\lambda_2) = \frac{e^{-\lambda_2}\lambda_2^{k_2}}{k_2!}. \tag{38}$$

Its log-likelihood function fixing discrete variable k_2:

$$l_2(\lambda_2;k_2) = \log[g_2(k_2|k_1;\lambda_2)] = -\lambda_2 + k_2\log\lambda_2 - \log k_2!, \tag{39}$$

with the parameter λ_2 reads:

$$\lambda_2 = E(k_2)e^{\alpha k_1 - [\exp(\alpha)-1]E(k_1)}. \tag{40}$$

For fixing continuous variable ν_2, we redefine the parameter λ_2 as:

$$\lambda_2 \equiv \rho_2(\lambda_2 - c_2 + \eta_2)e^{\alpha\nu_1 - [\exp(\alpha)-1]\rho_1(\lambda_1 - c_1 + \eta_1)}. \tag{41}$$

The log-likelihood function l_2 now become a function of two parameters λ_1, λ_2 fixing two variables ν_1, ν_2:

$$l_2(\lambda_1,\lambda_2;\nu_1,\nu_2) = -\lambda_2 + \nu_2\log\lambda_2 + \text{const.} \tag{42}$$

Its Δ log-likelihood function reads:

$$\Delta l_2(\lambda_1,\lambda_2;\nu_1,\nu_2) = l_2(\lambda_1,\lambda_2;\nu_1,\nu_2) - l_2(c_1,c_2;\nu_1,\nu_2). \tag{43}$$

The correlation in 34 becomes:

$$\text{Corr}(\nu_1,\nu_2) = \frac{\nu_1\nu_2[\exp(\alpha)-1]}{\sqrt{\nu_1\nu_2\{1+\nu_2\{e^{\nu_1[\exp(\alpha)-1]^2}-1\}\}}}. \tag{44}$$

Finally, the Δlog-likelihood for joint pmf:

$$\Delta l_{\text{join}}(\lambda_1,\lambda_2;\nu_1,\nu_2) = \Delta l_1(\lambda_1;\nu_1) + \Delta l_2(\lambda_1,\lambda_2;\nu_1,\nu_2). \tag{45}$$

References

[1] J. Bernon and B. Dumont, *Lilith: a tool for constraining new physics from Higgs measurements*, Eur. Phys. J. **C75**(9), 440 (2015), doi:10.1140/epjc/s10052-015-3645-9, 1502.04138.

[2] G. Aad *et al.*, *Measurements of the Higgs boson production and decay rates and constraints on its couplings from a combined ATLAS and CMS analysis of the LHC pp collision data at $\sqrt{s}$ = 7 and 8 TeV*, JHEP **08**, 045 (2016), doi:10.1007/JHEP08(2016)045, 1606.02266.

[3] A. M. Sirunyan *et al.*, *Combined measurements of Higgs boson couplings in proton–proton collisions at $\sqrt{s}$ = 13 TeV*, Eur. Phys. J. **C79**(5), 421 (2019), doi:10.1140/epjc/s10052-019-6909-y, https://cms-results.web.cern.ch/cms-results/public-results/publications/HIG-17-031/, 1809.10733.

[4] R. Barlow, *Asymmetric statistical errors*, In *Statistical Problems in Particle Physics, Astrophysics and Cosmology (PHYSTAT 05): Proceedings, Oxford, UK, September 12-15, 2005*, pp. 56–59 (2004), physics/0406120.

[5] P. Berkhout and E. Plug, *A bivariate Poisson count data model using conditional probabilities*, In *Statistica Neerlandica*, pp. 349–364 (2004).

[6] M. Aaboud *et al.*, *Measurements of Higgs boson properties in the diphoton decay channel with 36 fb^{-1} of pp collision data at $\sqrt{s} = 13$ TeV with the ATLAS detector*, Phys. Rev. **D98**, 052005 (2018), doi:10.1103/PhysRevD.98.052005, https://atlas.web.cern.ch/Atlas/GROUPS/PHYSICS/PAPERS/HIGG-2016-21/, 1802.04146.

[7] M. Aaboud *et al.*, *Measurement of the Higgs boson coupling properties in the $H \to ZZ^* \to 4\ell$ decay channel at $\sqrt{s}$ = 13 TeV with the ATLAS detector*, JHEP **03**, 095 (2018), doi:10.1007/JHEP03(2018)095, https://atlas.web.cern.ch/Atlas/GROUPS/PHYSICS/PAPERS/HIGG-2016-22/, 1712.02304.

[8] M. Aaboud *et al.*, *Measurements of gluon-gluon fusion and vector-boson fusion Higgs boson production cross-sections in the $H \to WW^* \to e\nu\mu\nu$ decay channel in pp collisions at $\sqrt{s} = 13$ TeV with the ATLAS detector*, Phys. Lett. **B789**, 508 (2019), doi:10.1016/j.physletb.2018.11.064, https://atlas.web.cern.ch/Atlas/GROUPS/PHYSICS/PAPERS/HIGG-2016-07, 1808.09054.

[9] M. Aaboud *et al.*, *Cross-section measurements of the Higgs boson decaying into a pair of τ-leptons in proton-proton collisions at $\sqrt{s} = 13$ TeV with the ATLAS detector*, Phys. Rev. **D99**, 072001 (2019), doi:10.1103/PhysRevD.99.072001, https://atlas.web.cern.ch/Atlas/GROUPS/PHYSICS/PAPERS/HIGG-2017-07, 1811.08856.

[10] M. Aaboud *et al.*, *Search for Higgs bosons produced via vector-boson fusion and decaying into bottom quark pairs in $\sqrt{s} = 13$ TeV pp collisions with the ATLAS detector*, Phys. Rev. **D98**(5), 052003 (2018), doi:10.1103/PhysRevD.98.052003, https://atlas.web.cern.ch/Atlas/GROUPS/PHYSICS/PAPERS/HIGG-2016-30, 1807.08639.

[11] M. Aaboud *et al.*, *Evidence for the $H \to b\bar{b}$ decay with the ATLAS detector*, JHEP **12**, 024 (2017), doi:10.1007/JHEP12(2017)024, https://atlas.web.cern.ch/Atlas/GROUPS/PHYSICS/PAPERS/HIGG-2016-29, 1708.03299.

[12] M. Aaboud *et al.*, *Search for an invisibly decaying Higgs boson or dark matter candidates produced in association with a Z boson in pp collisions at $\sqrt{s}$ = 13 TeV with the ATLAS detector*, Phys. Lett. **B776**, 318 (2018), doi:10.1016/j.physletb.2017.11.049, https://atlas.web.cern.ch/Atlas/GROUPS/PHYSICS/PAPERS/HIGG-2016-28/, 1708.09624.

[13] M. Aaboud *et al.*, *Evidence for the associated production of the Higgs boson and a top quark pair with the ATLAS detector*, Phys. Rev. **D97**(7), 072003 (2018), doi:10.1103/PhysRevD.97.072003, https://atlas.web.cern.ch/Atlas/GROUPS/PHYSICS/PAPERS/HIGG-2017-02, 1712.08891.

[14] M. Aaboud *et al.*, *Search for the standard model Higgs boson produced in association with top quarks and decaying into a $b\bar{b}$ pair in pp collisions at $\sqrt{s}$ = 13 TeV with the ATLAS detector*, Phys. Rev. **D97**(7), 072016 (2018), doi:10.1103/PhysRevD.97.072016, https://atlas.web.cern.ch/Atlas/GROUPS/PHYSICS/PAPERS/HIGG-2017-03, 1712.08895.

[15] A. M. Sirunyan *et al.*, *Search for invisible decays of a Higgs boson produced through vector boson fusion in proton-proton collisions at $\sqrt{s}$ = 13 TeV* (2018), doi:10.1016/j.physletb.2019.04.025, https://cms-results.web.cern.ch/cms-results/public-results/publications/HIG-17-023/, 1809.05937.

[16] A. M. Sirunyan *et al.*, *Search for the associated production of the Higgs boson and a vector boson in proton-proton collisions at $\sqrt{s}$ = 13 TeV via Higgs boson decays to τ leptons*, Submitted to: JHEP (2018), https://cms-results.web.cern.ch/cms-results/public-results/publications/HIG-18-007/, 1809.03590.

[17] A. M. Sirunyan *et al.*, *Measurements of Higgs boson properties in the diphoton decay channel in proton-proton collisions at $\sqrt{s}$ = 13 TeV*, JHEP **11**, 185 (2018), doi:10.1007/JHEP11(2018)185, 1804.02716.

[18] A. M. Sirunyan *et al.*, *Measurements of properties of the Higgs boson decaying into the four-lepton final state in pp collisions at $\sqrt{s}$ = 13 TeV*, JHEP **11**, 047 (2017), doi:10.1007/JHEP11(2017)047, 1706.09936.

[19] A. M. Sirunyan *et al.*, *Measurements of properties of the Higgs boson decaying to a W boson pair in pp collisions at $\sqrt{s}$ = 13 TeV*, Phys. Lett. **B791**, 96 (2019), doi:10.1016/j.physletb.2018.12.073, 1806.05246.

[20] A. M. Sirunyan *et al.*, *Observation of the Higgs boson decay to a pair of τ leptons with the CMS detector*, Phys. Lett. **B779**, 283 (2018), doi:10.1016/j.physletb.2018.02.004, 1708.00373.

[21] A. M. Sirunyan *et al.*, *Evidence for the Higgs boson decay to a bottom quark–antiquark pair*, Phys. Lett. **B780**, 501 (2018), doi:10.1016/j.physletb.2018.02.050, 1709.07497.

[22] A. M. Sirunyan *et al.*, *Inclusive search for a highly boosted Higgs boson decaying to a bottom quark-antiquark pair*, Phys. Rev. Lett. **120**(7), 071802 (2018), doi:10.1103/PhysRevLett.120.071802, 1709.05543.

[23] A. M. Sirunyan *et al.*, *Search for the Higgs boson decaying to two muons in proton-proton collisions at $\sqrt{s}$ = 13 TeV*, Phys. Rev. Lett. **122**(2), 021801 (2019), doi:10.1103/PhysRevLett.122.021801, 1807.06325.

[24] A. M. Sirunyan *et al.*, *Evidence for associated production of a Higgs boson with a top quark pair in final states with electrons, muons, and hadronically decaying τ leptons at $\sqrt{s} = 13$ TeV*, JHEP **08**, 066 (2018), doi:10.1007/JHEP08(2018)066, 1803.05485.

[25] A. M. Sirunyan *et al.*, *Search for* $\mathrm{t\bar{t}H}$ *production in the* $\mathrm{H} \to \mathrm{b\bar{b}}$ *decay channel with leptonic* $\mathrm{t\bar{t}}$ *decays in proton-proton collisions at* $\sqrt{s} = 13$ *TeV*, JHEP **03**, 026 (2019), doi:10.1007/JHEP03(2019)026, 1804.03682.

[26] A. M. Sirunyan *et al.*, *Search for* $\mathrm{t\bar{t}}H$ *production in the all-jet final state in proton-proton collisions at* $\sqrt{s} = 13$ *TeV*, JHEP **06**, 101 (2018), doi:10.1007/JHEP06(2018)101, 1803.06986.